

# Tensile performance of carbon-fibre-reinforced glass

V. C. NARDONE, K. M. PREWO

*United Technologies Research Center, East Hartford, Connecticut 06108, USA*

The tensile behaviour of unidirectional and  $[\pm\theta]_s$  angle-ply HMU carbon-fibre-reinforced borosilicate glass was determined as a function of the angle between the fibre and the applied load. Both the longitudinal and transverse strain of the composite are reported and discussed relative to the microstructural features responsible for the observed composite behaviour. Stress-strain behaviour for static and cyclic loading conditions is presented. The experimentally determined values of the composite elastic modulus and strength are also compared with those predicted from classical laminate theory. The composite tensile strength is accurately predicted by the Tsai-Hill failure criterion. The elastic modulus measurements indicate that the shear modulus of the uniaxially reinforced composites is higher than that of the multiaxially reinforced composites. This observation is attributed to more extensive matrix microcracking being present in the multiaxially reinforced composite as a result of fabrication. The failure modes present in the composite are also documented.

## 1. Introduction

The use of carbon fibres to reinforce glass matrices is part of an ongoing research effort to produce structurally performing ceramic matrix composites [1-6]. The carbon fibres act to increase the strength, modulus and toughness of the ceramic matrix, as well as providing improved wear resistance and excellent thermal stability. The purpose of the current investigation was to systematically determine the tensile stress-strain behaviour of a carbon-fibre-reinforced borosilicate glass composite for various unidirectional and angle-ply composite configurations. The primary variable investigated was the angle between the applied load axis and the fibre direction. The mechanistic basis for the composite stress-strain behaviour is established. In addition, values obtained for the composite modulus and tensile strength are compared with predictions by classical laminate theory [7].

## 2. Experimental procedure

All composites fabricated consisted of a borosilicate glass (Corning Glass Works 7740, Corning, New York) reinforced with Hercules HMU carbon fibres. The fabrication process involved impregnating the fibre by passing it through a glass powder slurry containing an organic binder while wrapping the fibre on a rotating drum. The impregnated fibre tape was in turn cut, stacked in the appropriate configuration, treated to remove binder and consolidated by vacuum hot-press densification.

A listing of the composite panel configurations fabricated along with their nominal fibre volume fractions is given in Table I. The 60° composite was fabricated at a lower fibre volume fraction because the higher fibre volume fraction material was too fragile to be accurately tested. The panel dimensions

were 5.08 cm × 12.7 cm and consisted of 8 laminate layers resulting in a panel thickness of approximately 0.2 cm. Representative examples of the composite microstructures are given in Figs 1 and 2.

Tensile specimens were cut from the panels using a diamond abrasive saw. Specimen dimensions were 12.7 cm in length and 1 cm in width, except for the 10° and  $[\pm 10]_s$  composites where the specimen width was 0.64 cm. Fibreglass doublers were adhesively bonded to the tensile specimens providing a gauge length of either 2.54 or 5.08 cm. The specimen dimensions were selected to ensure that continuous fibre paths to the specimen free edges occurred within the specimen gauge length. Strain was monitored using strain gauges mounted on both sides of the specimens. Tensile testing was conducted at a constant crosshead deflection rate of 0.0254 cm min<sup>-1</sup>. All testing was performed at room temperature with the specimens in the "as-fabricated" condition. In some cases, specimens were loaded to approximately half their ultimate tensile strength, unloaded, and subsequently reloaded to failure.

TABLE I HMU carbon-fibre-reinforced 7740 borosilicate glass matrix composites fabricated for analysis of stress-strain behaviour

Fibre orientation	Nominal fibre $V_f$ (%)
0°	43.6
10°	43.6
30°	43.0
60°	30.0
$[\pm 10]_s$	42.3
$[\pm 30]_s$	42.3
$[\pm 45]_s$	42.8
$[\pm 60]_s$	42.3
$[0/90]$	40.1

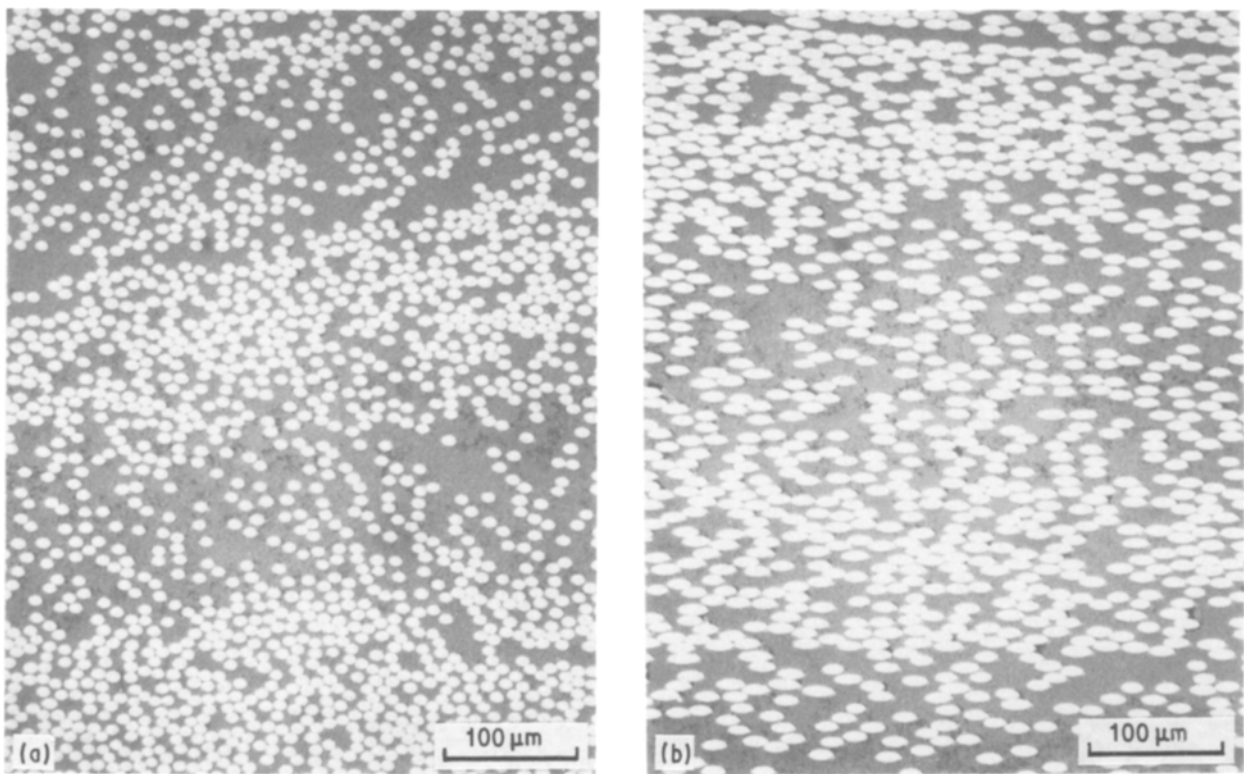


Figure 1 Optical micrographs of a 30° unidirectional HMU-7740 composite cross-section: (a) longitudinal, (b) transverse.

### 3. Experimental results

#### 3.1. Unidirectional composite data

Typical stress-strain behaviour of a 0° unidirectional composite is presented in Fig. 3. Both the longitudinal (parallel to the fibres) and transverse strains are shown as a function of axial applied stress. Initially the longitudinal curve is linear, followed by a region of increased strain with very little increase in stress. The transverse strain of the composite has a positive

component. Note that the maximum positive transverse strain rate coincides with the maximum positive longitudinal strain rate.

Unidirectional composite stress-strain behaviour as a function of  $\theta$ , the angle between load axis and the fibre direction, is given in Fig. 4. For the 10° and 30° composites, the stress-strain behaviour is nearly linear to fracture. In addition, the transverse strain (not shown) remained negative and linear to fracture. Note

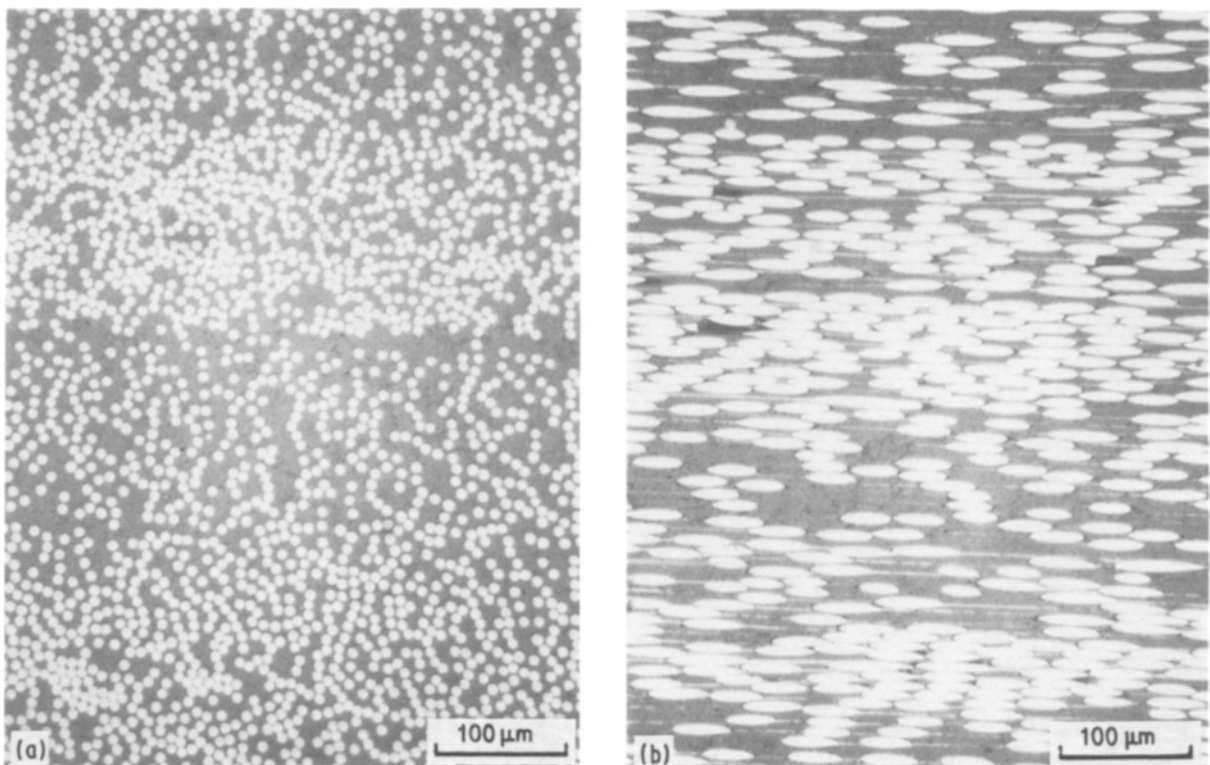


Figure 2 Optical micrographs of a  $[\pm 10]_s$  angle-ply HMU-7740 composite cross-section: (a) longitudinal, (b) transverse.

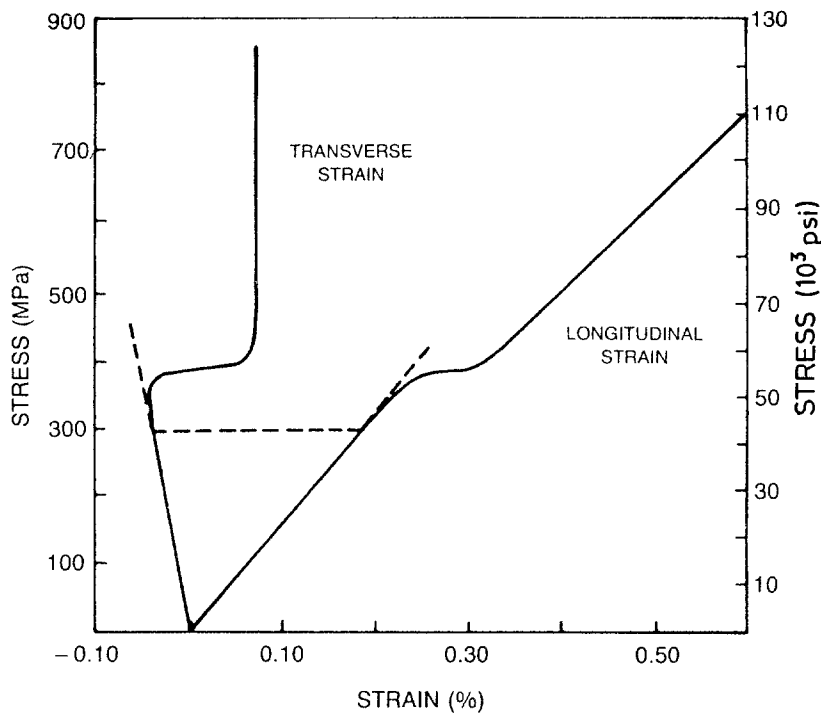


Figure 3 Longitudinal and transverse strain against applied tensile load for 0°-43 vol % HMU-7740 composites.

the dramatic loss of modulus and strength with increasing values of  $\theta$ .

Representative examples of unidirectional composite stress against longitudinal strain that involves cyclic loading are shown in Figs 5 and 6. When loading past the proportional limit of a 0° specimen, a positive residual offset remains after unloading. For the specimen in Fig. 5, the magnitude of this offset is about  $500 \mu\epsilon$  ( $1 \mu\epsilon = 0.0001\%$ ). On subsequent reloading, the composite stress-strain behaviour is essentially linear until the maximum load of the initial loading cycle is exceeded, when a slight inflection in the stress-strain behaviour is evident. For the case of

the 10° sample shown in Fig. 6, unloading results in no residual strain offset. Subsequent reloading follows the initial stress-strain curve. Similar linear behaviour is observed for the 0° sample when the initial loading segment remains below the knee of the curve.

The effect of cyclic loading on the transverse strain of the 0° unidirectional composite is shown in Fig. 7. The transverse strain shown in Fig. 7 was measured on the same specimen used to generate the longitudinal strain shown in Fig. 5. Note that the second loading has much less positive strain accumulation relative to the initial loading.

A summary of all the tensile data generated for the

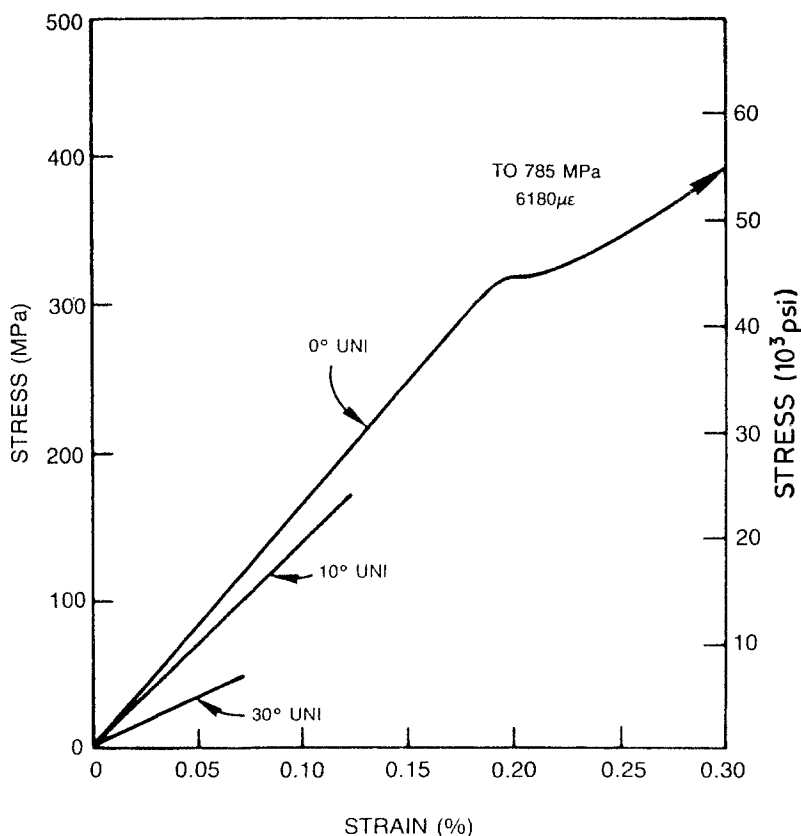


Figure 4 Longitudinal strain against applied tensile load for unidirectional 43 vol % HMU-7740 composites.

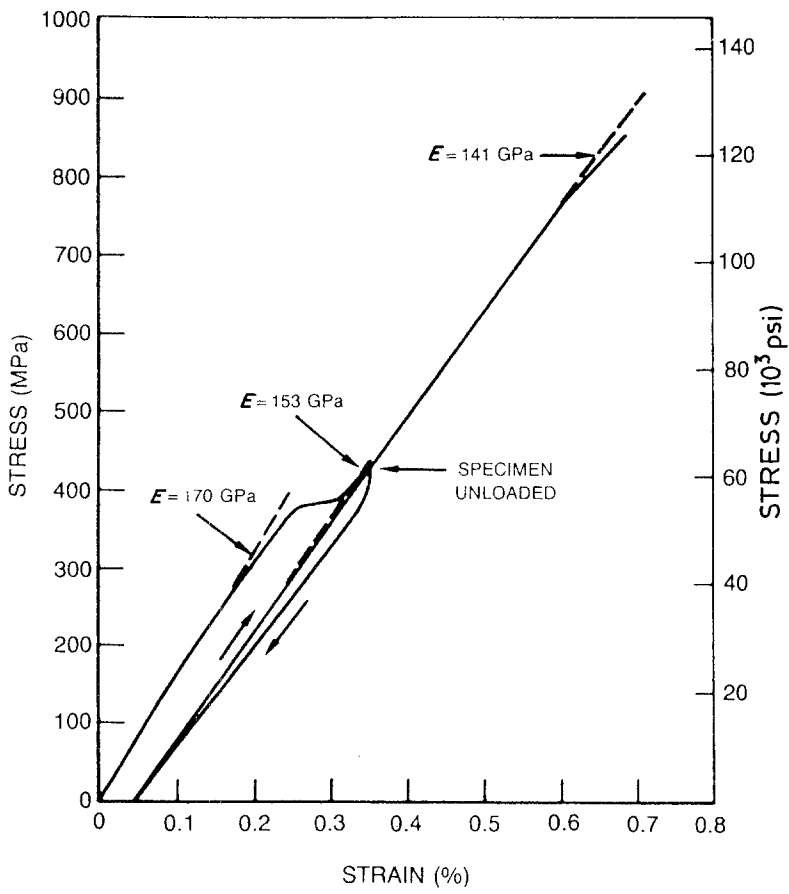


Figure 5 Applied stress against longitudinal strain for 0°-43 vol% HMU-7740 composites under cyclic loading conditions.

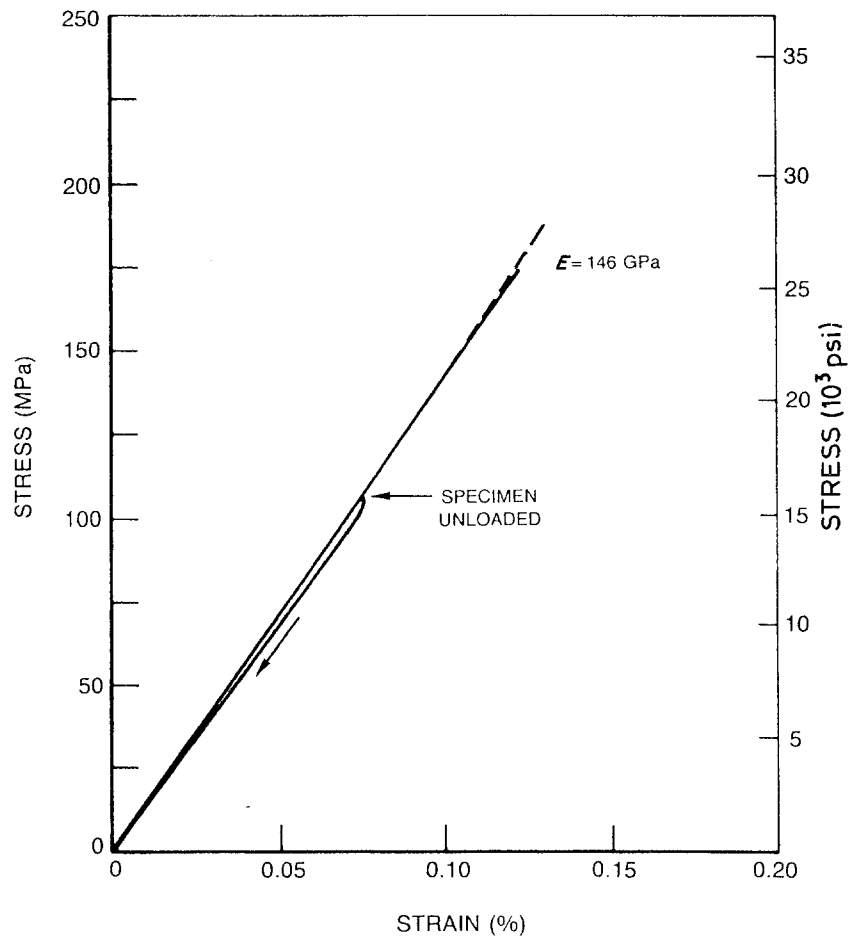


Figure 6 Applied stress against longitudinal strain for 10°-43 vol% HMU-7740 composites under cyclic loading conditions.

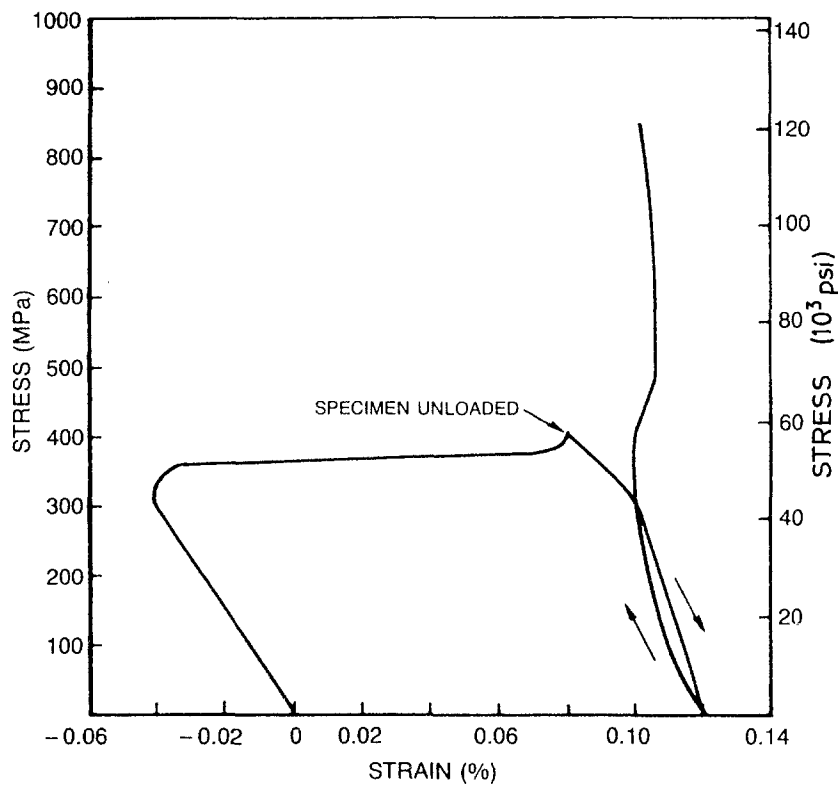


Figure 7 Applied stress against transverse strain for 0°-43 vol % HMU-7740 composites under cyclic loading conditions.

unidirectional composites is given in Table II. Photographs of representative tensile failures are shown in Fig. 8.

### 3.2. Multiaxially reinforced composite data

Typical stress-strain behaviour of the multiaxially reinforced ( $\pm\theta$ ) composites is given in Fig. 9, along with a 0° unidirectional sample for comparison. Only a limited linear region is evident for the  $\pm\theta$  (angle-ply) composites, with the fraction of the linear region of the stress-strain curve decreasing with increasing values of  $\theta$ . Fig. 10 shows both the longitudinal and transverse strains as a function of stress for the  $[\pm 10]_s$  composite and Fig. 11 for the  $[0/90]$  composite. In

both the  $[\pm 10]_s$  and  $[0/90]$  composite samples, positive transverse strain was measured as reported above for the 0° sample. A comparison of the magnitude of the positive transverse strains for all composites exhibiting such behaviour is given in Table III.

A representative example of stress against longitudinal strain that involves cyclic loading is given in Fig. 12. The effect of cyclic loading on the transverse strain behaviour of the  $[\pm 10]_s$  composite is shown in Figs 13 and 14. In Fig. 13, the initial applied load is only slightly greater than the composite proportional limit while in Fig. 14 the initial applied load is substantially greater than the composite proportional limit. The second loading cycle in Fig. 13 shows a much greater amount of positive strain relative to Fig. 14. A summary of the tensile data generated for the angle-ply composites is given in Table IV. Photographs of representative angle-ply tensile failures are given in Fig. 15.

TABLE II Summary of unidirectional composite tensile data\*

Composite	$E$ (GPa)	PL (MPa)	UTS (MPa)	$\nu$	$\epsilon_f$ (%)
0°	165	299	787	0.170	0.618
	170	266	856	0.195	0.657
	173	304	711	0.183	0.531
Mean value	169	290	785	0.183	0.602
10°	129	139	170	0.184	0.123
	146	128	175	0.198	0.121
	144	153	168	0.179	0.111
Mean value	140	140	171	0.187	0.118
30°	72	29	50	0.169	0.078
	70	41	50	0.197	0.073
	68	39	41	0.187	0.060
Mean value	70	37	47	0.184	0.070
60°	35	11	18	0.112	0.054
	38	16	28	0.134	0.075
	33	19	24	0.086	0.077
Mean value	35	15	23	0.111	0.069

\*  $E$  = Elastic modulus taken as the slope of the stress-strain curve up to the PL; PL = proportional limit taken as the initial deviation from linearity of the stress-strain curve; UTS = ultimate tensile strength taken as the ultimate load divided by the original cross-sectional area;  $\nu$  = Poisson's ratio;  $\epsilon_f$  = ultimate failure strain.

## 4. Discussion

### 4.1. Tensile stress-strain behaviour

The stress-strain behaviour of a 0° unidirectional sample is illustrated in Fig. 3. There is a large component of positive transverse strain that corresponds to the "knee" of the longitudinal stress-strain curve.

TABLE III Tensile transverse strain behaviour of unidirectional and angle-ply composites\*

Composite	Magnitude of positive transverse strain component (%)
0°	0.12
$[\pm 10]_s$	0.06
$[0/90]$	0.005

\* All composites not reported had no positive transverse strain component.

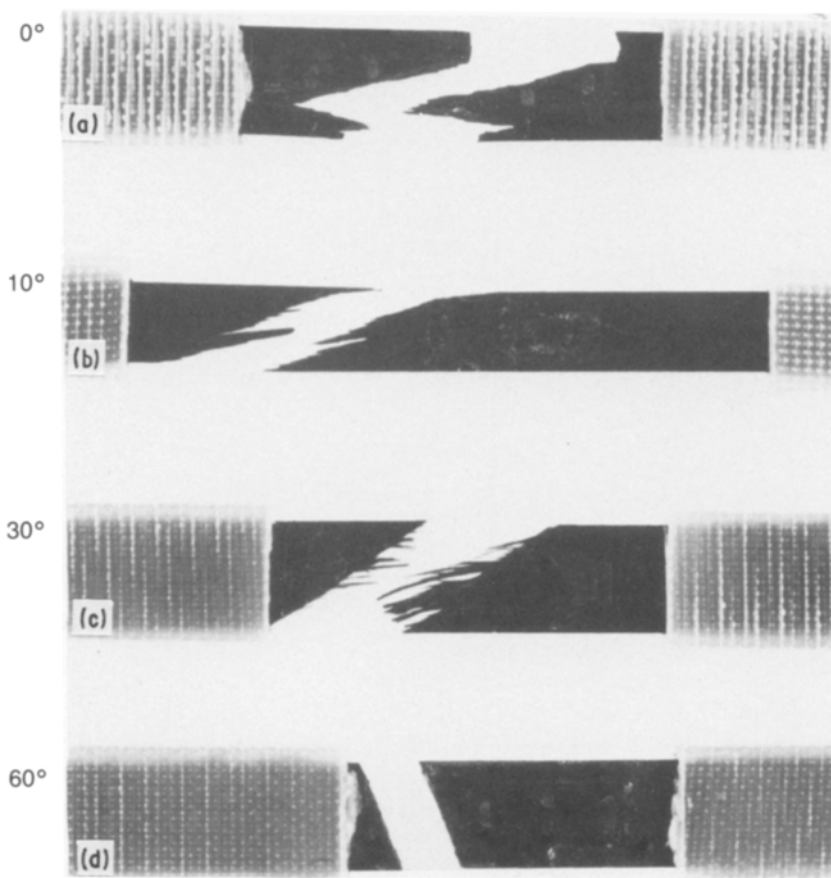


Figure 8 Characteristic failure modes of the HMU-7740 unidirectional tensile samples: (a) 0°, (b) 10°, (c) 30°, (d) 60°.

The knee in the stress-strain curve is due to the onset of matrix microcracking. Apparently, as the matrix goes through the process of microcracking, the fibres are no longer constrained and they tend to “broom out” so as to increase the average interfibre spacing. This in turn results in the positive component of the transverse strain. Note that for both the longitudinal and transverse strains shown in Fig. 3, the high rate of positive strain accumulation occurs over a limited stress range.

For the other orientations, the transverse strain showed no indication of possessing positive components. As shown in Fig. 4 for the 10° and 30° composites, the longitudinal stress-strain curve is nearly linear to fracture. This may be attributed to the fact that composite failure occurs prior to the point of substantial matrix microcracking. Since very little matrix microcracking occurs in these off-axis unidirectional composites, there is no driving force for the accumulation of positive transverse strain.

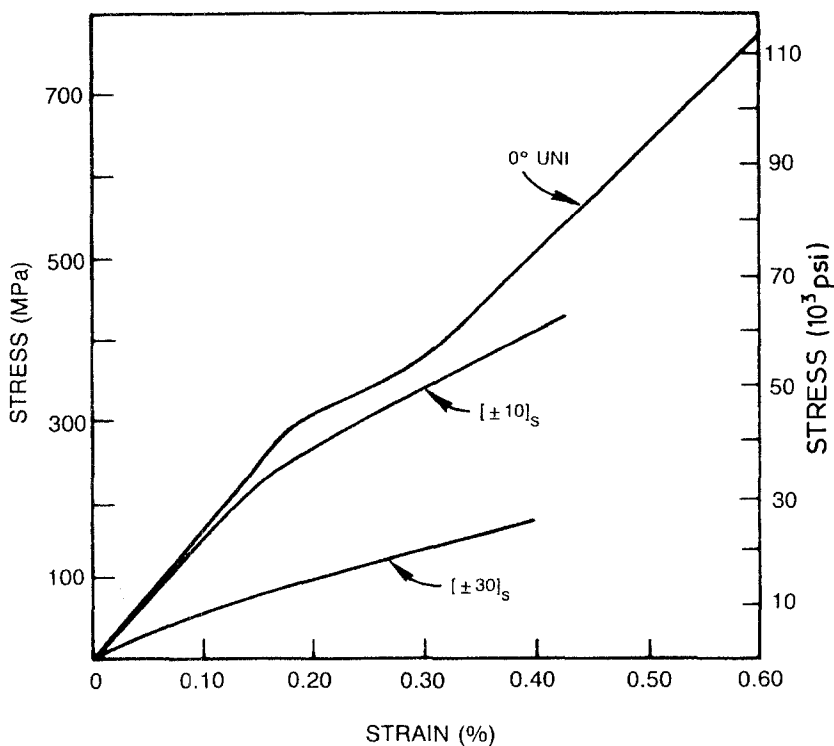


Figure 9 Longitudinal strain as a function of applied load for 43 vol % HMU-7740 composites.

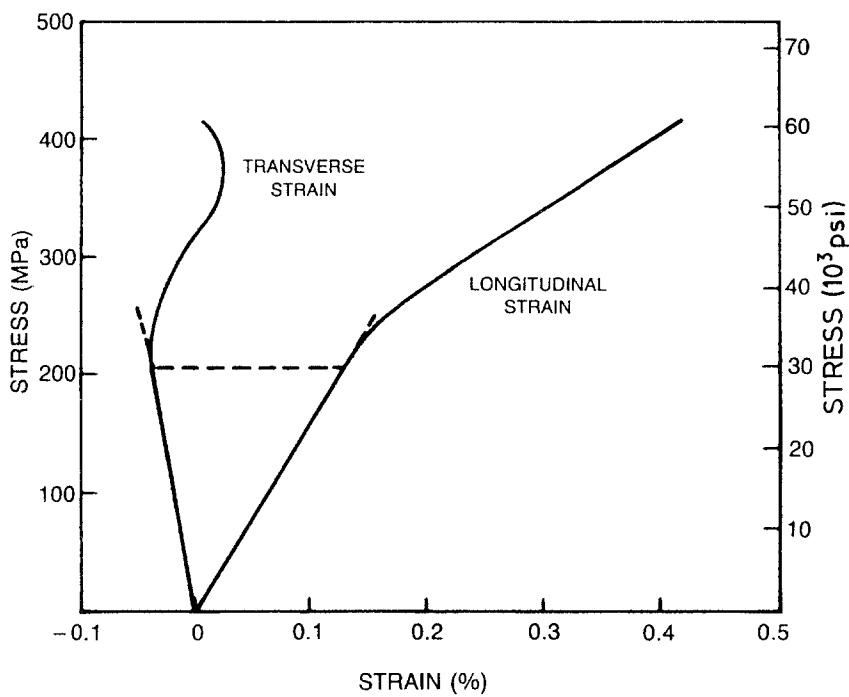


Figure 10 Longitudinal and transverse strain against applied tensile load for  $[\pm 10]_s$ -42 vol % HMU-7740 composites.

For the case of the multiaxially reinforced composites, where the stress-strain behaviour is illustrated in Figs 10 and 11, both the rate and magnitude of positive transverse strain accumulation are decreased relative to the  $0^\circ$  sample. This may be explained primarily by three factors. First, the longitudinal strain of the multiaxially reinforced composites shows a much more gradual and extended region of non-linear behaviour. It may therefore be inferred that the process of matrix microcracking occurs over a greater fraction of the composite stress-strain curve. This would tend to decrease the rate at which positive transverse strain is accumulated during any given portion of the stress-strain curve, and cause it to be somewhat masked by the usual Poisson (negative)

transverse strain. The second principal factor that comes into play results from the individual composite plies being oriented in different directions. For example, in the  $[0/90]$  composite the adjacent plies are oriented at  $90^\circ$  to one another. This will tend to restrain the positive transverse strain that occurs in any given ply, thus decreasing the magnitude of the strain relative to the  $0^\circ$  sample. A final factor that affects the magnitude of the positive transverse strain arises from geometrical considerations. Assuming that the brooming out of the fibres that occurs during matrix microcracking results in a positive transverse strain component perpendicular to the fibre direction, the resolved positive transverse strain will decrease as the value of  $\theta$  increases.

There was no positive transverse strain component measured for the  $[\pm 30]_s$ ,  $[\pm 45]_s$  or  $[\pm 60]_s$  composites, even though matrix microcracking occurs as evidenced by highly non-linear longitudinal stress-strain behaviour. This may be anticipated, since all of the factors identified above that tend to inhibit the accumulation of positive transverse strain become more prominent as the value of  $\theta$  increases in  $[\pm \theta]_s$  composites.

TABLE IV Summary of angle-ply composite tensile data\*

Composite	$E$ (GPa)	PL (MPa)	UTS (MPa)	$\nu$	$\epsilon_f$ (%)
$[\pm 10]_s$	158	170	429	0.286	0.420
	161	160	469	0.269	0.418
	163	224	424	0.295	0.391
Mean value	161	185	441	0.283	0.410
$[\pm 30]_s$	81	12	179	0.887	0.399
	70	19	193	0.834	0.524
	77	14	189	0.972	0.594
Mean value	76	15	187	0.898	0.506
$[\pm 45]_s$	42	5.6	44	0.696	0.384
	35	5.6	40	0.687	0.249
	36	6.6	48	0.633	0.512
Mean value	38	5.9	44	0.672	0.382
$[\pm 60]_s$	24	3.0	25	0.287	0.655
	24	2.8	25	0.313	0.408
	20	4.5	22	0.248	0.459
Mean value	23	3.4	24	0.283	0.507
$[0/90]$	81	39	252	0.022	0.403
	80	52	317	0.005	0.500
	86	39	331	0.025	0.527
Mean value	82	43	300	0.017	0.477

\*For definitions see Table II.

#### 4.2. Stress-strain behaviour involving load cycling

The effect of load cycling on the stress-longitudinal strain behaviour of the  $0^\circ$  unidirectional sample is shown in Fig. 5. After loading past the knee of the curve, unloading results in a positive residual strain offset. The magnitude of the strain offset is similar to the strain accumulated in the knee of the stress-strain curve. Subsequent reloading results in linear behaviour up to the maximum load value of the initial loading segment. The modulus that one measures from the second loading curve is decreased relative to the initial loading segment. For the example shown in Fig. 5, the modulus decreases from a value of 170 GPa to 153 GPa. On further loading past the maximum stress value of the initial load cycle, there is a slight

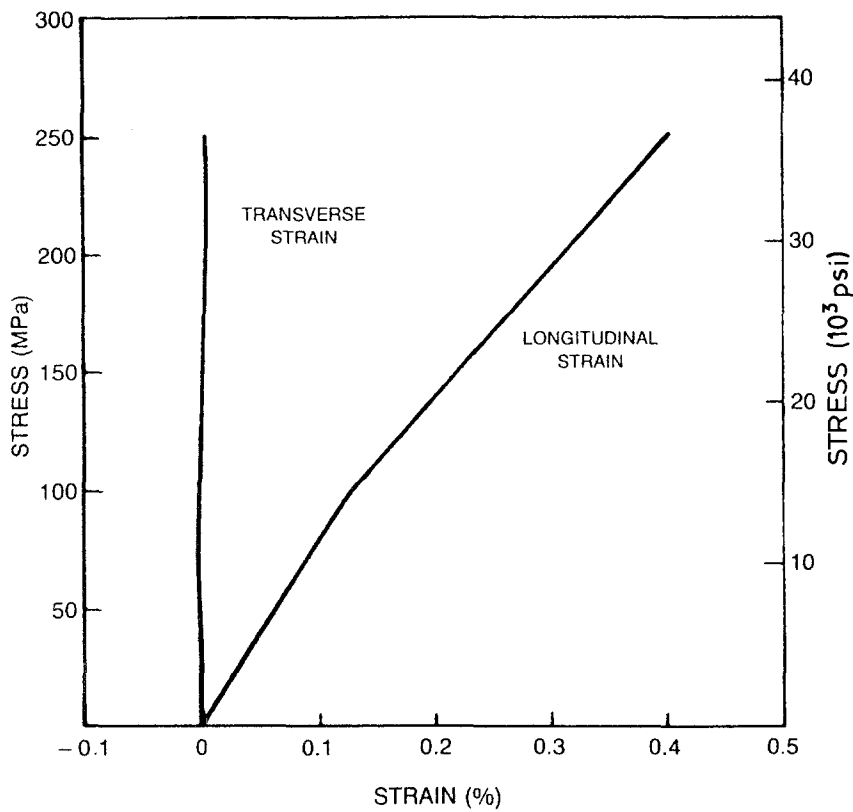


Figure 11 Longitudinal and transverse strain against applied tensile load for [0/90]-40 vol% HMU-7740 composites.

inflection and the modulus is further decreased to 141 GPa. This decrease in modulus can be attributed to the matrix microcracking, since the stiffness contribution provided by the matrix goes to nearly zero after extensive microcracking occurs. A quantitative measure of this effect can be estimated by multiplying the matrix volume fraction (0.56) by the matrix modulus (63 GPa), which results in an estimated decrease in modulus of 35 GPa. This compares favourably with the measured decrease of 29 GPa.

For all of the off-axis unidirectional samples tested,

unloading results in no measurable residual offset strain. Subsequent reloading follows the path of the first loading cycle (see Fig. 6). This is due to the fact that very little matrix microcracking occurs during the tensile testing of the off-axis composites, such that near-linear stress-strain behaviour is observed.

The transverse strain behaviour of the  $0^\circ$  unidirectional composite is shown in Fig. 7. The initial load application was beyond the knee of the stress-longitudinal strain curve (see Fig. 5). On unloading, a positive residual transverse strain of approximately

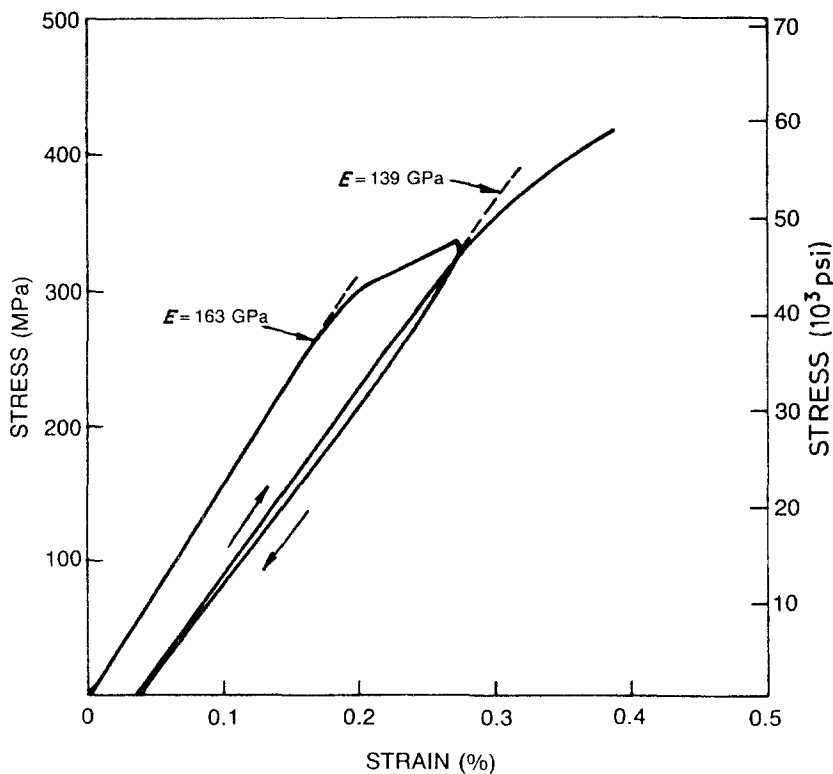


Figure 12 Applied stress against longitudinal strain for  $[\pm 10]_s$ -42 vol% HMU-7740 composites under cyclic loading conditions (high initial applied load).

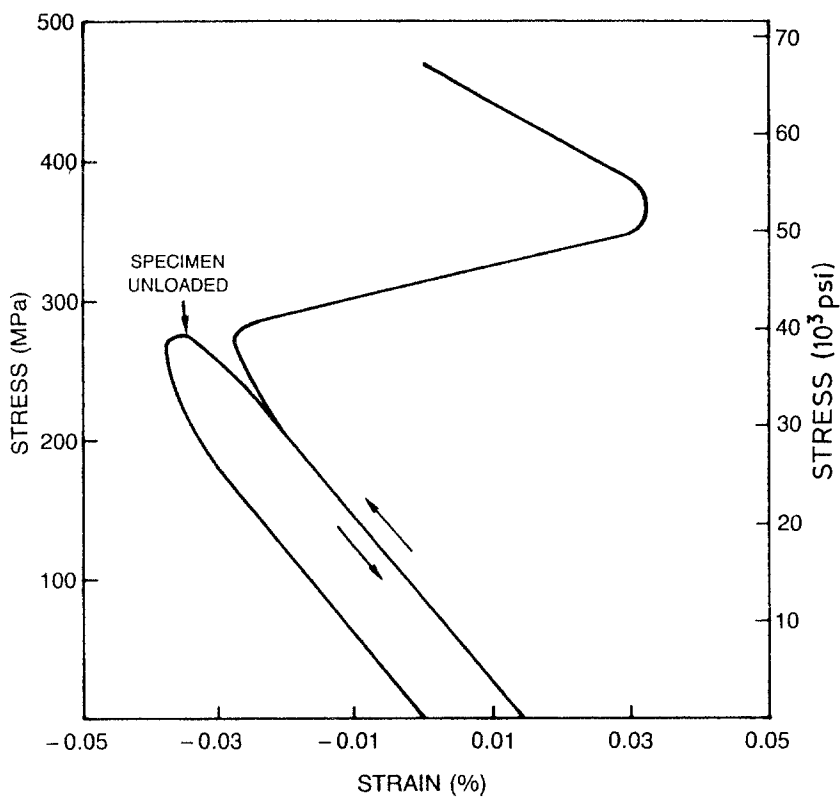


Figure 13 Applied stress against transverse strain for  $[\pm 10]_0$ -42 vol% HMU-7740 composites under cyclic loading conditions (low initial applied load).

1200  $\mu\epsilon$  was apparent. On subsequent reloading, very little transverse strain ( $< 200 \mu\epsilon$ ) either positive or negative is apparent. Evidently the positive strain accumulation due to matrix microcracking was exhausted during the initial load application.

For the case of the angle-ply composites, loading past the proportional limit results in a positive longitudinal residual strain offset after unloading (see Fig. 12). As was the case with the  $0^\circ$  unidirectional sample, this strain offset may be attributed to matrix microcracking. On subsequent reloading, the composite stress-strain behaviour has lost a large fraction of the non-linear component for loads up to the maximum load of the initial loading segment. Once the maximum load is exceeded, non-linear behaviour

occurs to a greater extent, due to additional matrix microcracking being induced by the higher load levels. The confirmation of extensive matrix microcracking during the load cycling is the decrease in modulus illustrated in Fig. 12.

A somewhat different situation is evident for the transverse strain during load cycling as shown in Figs 13 and 14. Even after extensive microcracking has occurred during the initial load application, as evidenced by a positive transverse strain component (see Fig. 14), the initial linear region of the stress-strain curve has the same slope for both loadings. This is in contrast to the longitudinal strain, where a decrease in modulus was apparent for the second load application. The reason for this difference may be due

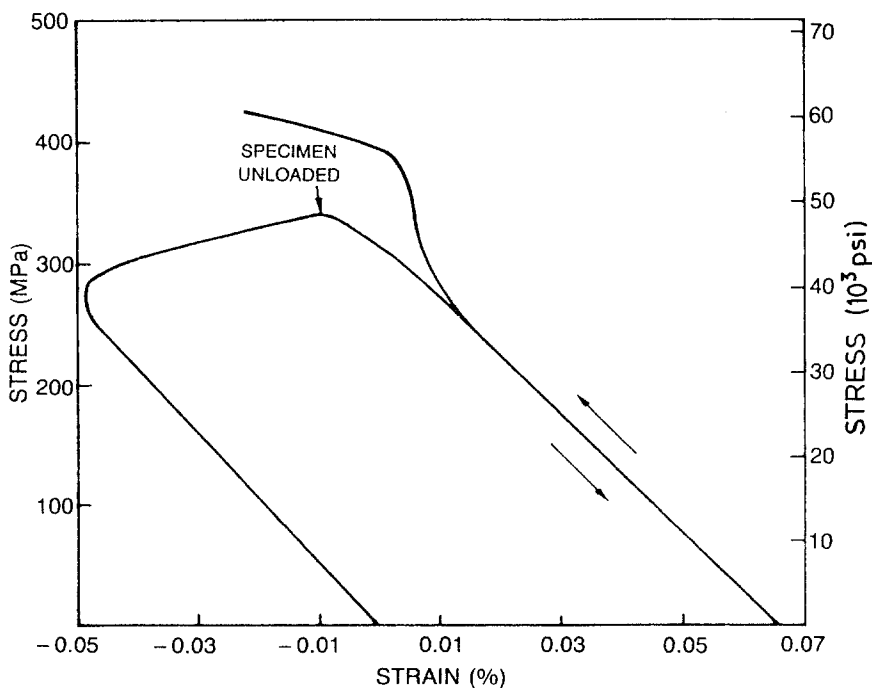


Figure 14 Applied stress against transverse strain for  $[\pm 10]_0$ -42 vol% HMU-7740 composites under cyclic loading conditions (high initial applied load).

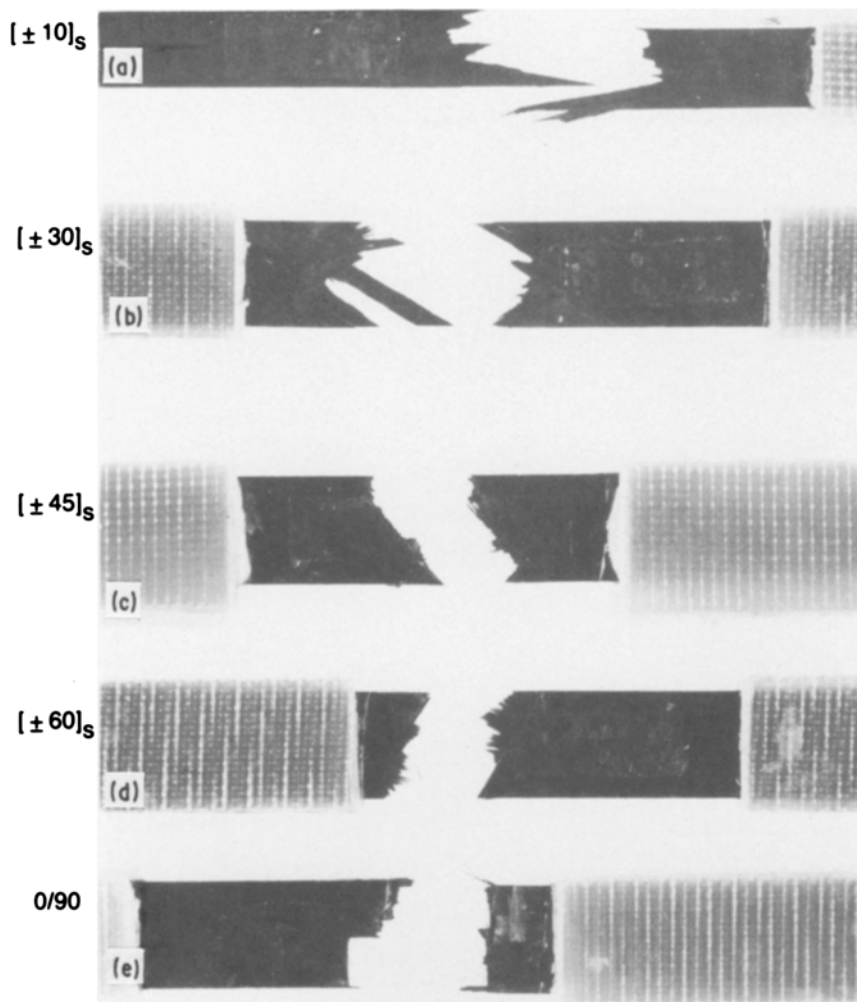


Figure 15 Characteristic failure modes of the angle-ply HMU-7740 tensile samples: (a)  $[\pm 10]_s$ , (b)  $[\pm 30]_s$ , (c)  $[\pm 45]_s$ , (d)  $[\pm 60]_s$ , (e) 0/90.

to the initial negative slope of the transverse strain being compressive due to Poisson contraction, while the longitudinal strain results from tensile loading. The influence of microcracking that occurred during the initial load application is anticipated to be much more prevalent for tensile relative to compressive loading. Thus, microcracking affects the slope of the linear portion of the stress against longitudinal strain curve during the second loading but has a minimal effect on the slope of the linear portion of the stress against transverse strain curve.

#### 4.3. Modulus and strength prediction

Classical laminate theory [7] was used to predict composite elastic modulus as a function of  $\theta$ . The results are summarized in Fig. 16, with the average data points from Tables II and IV being plotted. The values used for the composite longitudinal modulus (169 MPa) and Poisson's ratio (0.18) are the experimentally determined values from Table II. The value for the transverse modulus (21 MPa) was estimated from the higher- $\theta$  modulus values, while the value for the composite shear modulus ( $G_{12}$ ) was used as an adjustable parameter to fit the data. In order to successfully fit the composite elastic modulus data, the value for  $G_{12}$  of the off-axis unidirectional composites must be twice that of the value used for the  $[\pm \theta]_s$  angle-ply composites. The reason for the lower effective shear modulus in the angle-ply relative to the unidirectional composites may be attributed to matrix

microcracking. Cooling from fabrication temperatures results in the generation of residual stresses due to the difference in thermal expansion between the fibre and matrix. In angle-ply composites, additional residual stresses are generated due to ply anisotropy in thermal expansion. This increased residual stress causes more matrix microcracking in the angle-ply composites, and therefore the effective value for  $G_{12}$  is reduced.

One can also calculate the value for  $G_{12}$  from the following equation [7]:

$$\frac{1}{G_{12}} = \frac{V_m}{G_m} + \frac{V_f}{G_f} \quad (1)$$

where  $V_m$  is the matrix volume fraction (0.57),  $V_f$  is the fibre volume fraction (0.43),  $G_m$  is the matrix shear modulus (25 GPa) and  $G_f$  is the fibre shear modulus (28 GPa [7]). The calculated value of the shear modulus is 26 GPa, which compares favourably with the best-fit value for the unidirectional composites of 22 GPa. This result suggests that only a small amount of matrix microcracking is present in the as-fabricated unidirectional composites, with much more microcracking being present in the as-fabricated angle-ply composites.

Two different strength theories were considered for predicting composite strength as a function of  $\theta$ . These are the maximum-stress failure criterion and the Tsai-Hill (maximum-work) failure criterion. In the maximum-stress failure criterion, failure is assumed to

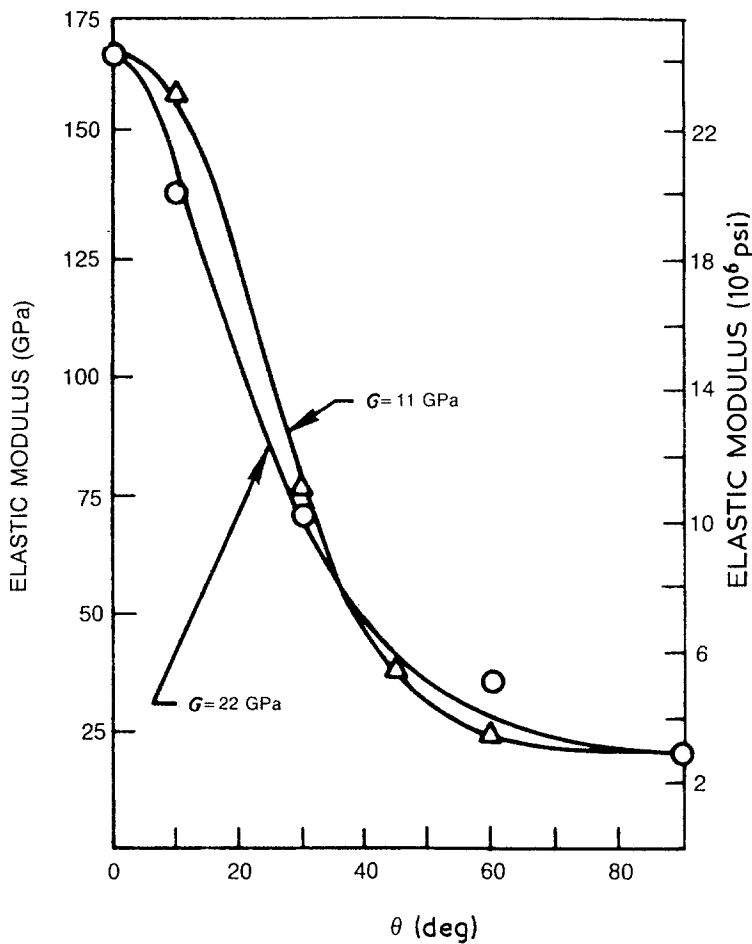


Figure 16 Comparison of measured and calculated elastic modulus values for (O) unidirectional and ( $\Delta$ ) angle-ply 43 vol % HMU-7740 composites.  $G_{\text{cal}} = 26$  GPa.

occur by one of three distinct mechanisms: tensile fibre failure, shear failure of the fibre–matrix interface or the matrix, and tensile failure of the fibre–matrix interface or the matrix [8–10]. For the case of a unidirectional composite, the applied stress ( $\sigma_{\text{APP}}$ ) necessary to cause tensile fibre failure is

$$\sigma_{\text{APP}} = \sigma_0 / \cos^2 \theta \quad (2)$$

where  $\sigma_0$  is the failure stress of a  $0^\circ$  composite for loading parallel to the fibre direction and  $\theta$  is the angle between the fibre axis and the applied load. The applied load necessary to cause shear failure is

$$\sigma_{\text{APP}} = \tau / (\sin \theta \cos \theta) \quad (3)$$

where  $\tau$  is the lesser of the fibre–matrix shear strength or the matrix shear strength. Finally, tensile failure of the fibre–matrix interface or matrix occurs when

$$\sigma_{\text{APP}} = \sigma_{90} / \sin^2 \theta \quad (4)$$

where  $\sigma_{90}$  is the tensile strength of the composite when the fibres are oriented at  $90^\circ$  to the applied stress.

Equations 2 to 4 may be used to predict unidirectional composite strength in two different manners. The maximum-stress theory predicts that the strength of the composite will be the least of the values for  $\sigma_{\text{APP}}$  in Equations 2 to 4 [8–10]. Alternatively, Equations 2 to 4 may be incorporated into Hill's maximum-work theory [11] for the yielding of an anisotropic material, as shown by Tsai. When this is done, the composite is predicted to fail [12, 13] when

$$\frac{1}{\sigma_{\text{APP}}^2} = \frac{\cos^4 \theta}{\sigma_0^2} + \left( \frac{1}{\tau^2} - \frac{1}{\sigma_0^2} \right) \cos^2 \theta \sin^2 \theta + \frac{\sin^4 \theta}{\sigma_{90}^2} \quad (5)$$

Both the maximum stress and Tsai–Hill theories have been used to successfully predict unidirectional resin matrix composite strength.

For the case of angle-ply composites, the Tsai–Hill theory predicts failure when

$$\frac{\sigma_x^2 - \sigma_x \sigma_y}{\sigma_0^2} + \frac{\sigma_y^2}{\sigma_{90}^2} + \frac{\sigma_s^2}{\tau^2} = 1 \quad (6)$$

where  $\sigma_x$  is the stress acting parallel to the fibres,  $\sigma_y$  is the stress acting perpendicular to the fibres and  $\sigma_s$  is the shear stress. Note that Equation 6 is simply a more general form for Equation 5. The values for  $\sigma_x$ ,  $\sigma_y$  and  $\sigma_s$  can be calculated from laminate theory [7].

The value assumed for  $\sigma_0$  (787 MPa) is taken from Table II, while the value for  $\sigma_{90}$  (17 MPa) was estimated from the higher- $\theta$  strength values. The value for  $\tau$  was used as an adjustable parameter to provide a best fit of the unidirectional data. For the case of the maximum-stress failure criterion, the value of  $\tau$  necessary to fit the unidirectional data is 25 MPa. However, the agreement between the actual and predicted strength values is relatively poor for both the unidirectional and angle-ply composites as shown in Table V. This is particularly so for  $\theta$  values of 10 and 30. In contrast, a very good prediction of strength is obtained when using the Tsai–Hill failure criteria and a value for  $\tau$  of 32 MPa. This is shown in Table V and graphically in Fig. 17. For the composites investigated here, the Tsai–Hill failure criterion provides a much better fit to the experimental data relative to the maximum-stress failure criterion. It is interesting to note that, unlike for the shear modulus, the same value of shear strength can be used for both

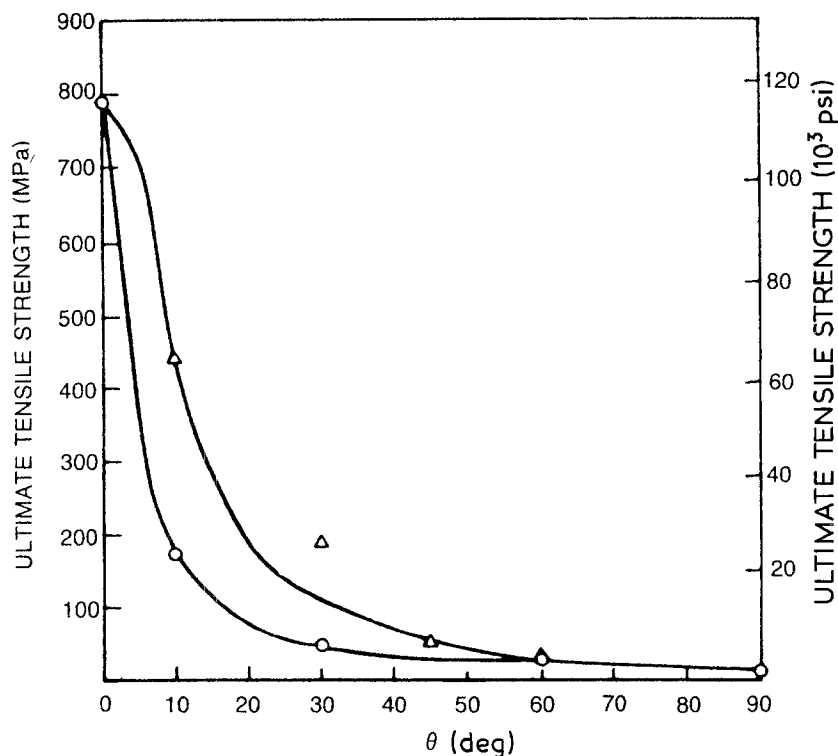


Figure 17 Comparison of measured and predicted strength of (O) unidirectional and ( $\Delta$ ) angle-ply 43 vol % HMU-7740 composites (Tsai-Hill failure criterion).

unidirectionally and multidirectionally reinforced composites. This may indicate that the shear strength of the composite is controlled by the fibre-matrix interfacial strength, such that matrix microcracking does not appreciably affect the composite shear strength.

#### 4.4. Failure modes

Typical failure modes for the unidirectional and angle-ply composites are shown in Figs 8 and 15. An interesting point to note is that the fracture surfaces do not display a pure shear failure mode, even for the off-axis unidirectional samples. In general, there are both regions of shear failure and regions of fibre failure. In the unidirectional composites, the fibre-failure regions show evidence of separation and rotation to the applied stress axis. In the angle-ply composites, there appears to be tensile fibre failure in the central portion of the specimen.

The failure modes exhibited by the composites are consistent with the maximum-stress failure criterion not accurately predicting composite strength. The theory assumes there are three distinct failure regions, i.e. tensile fibre failure, shear failure and tensile fibre-

matrix interface failure. In contrast, the observed failure modes are a mixture of these aforementioned failure regions.

#### 5. Conclusions

1. The stress-strain behaviour of HMU-7740 composites is highly non-linear, with the non-linearity being due to matrix microcracking.

2. Positive transverse strain components are evident during tensile testing of  $0^\circ$ ,  $[\pm 10]_s$  and  $[0/90]$  HMU-7740 composites. This behaviour is attributed to the carbon fibres tending to broom out as the matrix microcracks.

3. The observed magnitude of the positive transverse strain depends on the stress range where matrix microcracking occurs and the orientation of the plies relative to the applied stress axis.

4. For tensile testing involving load cycling, near-linear stress-strain behaviour is apparent for subsequent testing up to the maximum load of the initial load cycle, but a lower elastic modulus is apparent.

5. The calculated shear modulus of the multiaxially reinforced composite is less than that of a corresponding uniaxially reinforced composite. The behaviour is attributed to more extensive matrix microcracking being present in the multiaxially reinforced composites as a result of fabrication.

6. The Tsai-Hill failure criterion accurately predicts the strength of HMU-7740 composites.

7. The failure modes of the HMU-7740 composites are a mixture of tensile fibre failure and fibre-matrix interface failure.

#### Acknowledgements

We gratefully acknowledge the support of the Office of Naval Research (Contract N00014-85-C-0332) in performing this research under the monitorship of Dr Steven Fishman.

TABLE V Comparison of actual and predicted composite ultimate tensile strength

Composite	Experimental UTS (MPa)	Predicted maximum-stress UTS (MPa)*	Predicted Tsai-Hill UTS (MPa)†
$0^\circ$	787	787	787
$10^\circ$	171	145	176
$30^\circ$	47	57	51
$60^\circ$	23	23	22
$[\pm 10]_s$	440	759	425
$[\pm 30]_s$	187	106	109
$[\pm 45]_s$	44	50	59
$[\pm 60]_s$	24	28	26

\* Using  $\tau = 25$  MPa.

† Using  $\tau = 32$  MPa.

## References

1. K. M. PREWO and J. F. BACON, in Proceedings of 2nd International Conference on Composites, Vol. 1, edited by B. Noton *et al.*, Toronto, 16–20 April, 1978 (AIME, New York, 1978) pp. 64–74.
2. K. M. PREWO, J. F. BACON and E. R. THOMPSON, in Proceedings of AIME Conference on Advanced Fibres and Composites for Elevated Temperatures, edited by I. Ahmad and B. Noton, New Orleans, 20–21 February, 1979 (AIME, New York, 1979) pp. 80–93.
3. K. M. PREWO and E. R. THOMPSON, “Research on Graphite Reinforced Glass Matrix Composites”, NASA Contract Report 165711 (NASA, Washington, D.C., 1981).
4. K. M. PREWO, J. F. BACON and D. L. DICUS, *SAMPE Q.* **10** (4) (1979) 42.
5. E. MINFORD and K. PREWO, *Wear* **102** (1985) 253.
6. K. M. PREWO and E. J. MINFORD, *Proc. SPIE — Int. Soc. Opt. Engngs* **505** (August 1984) 188.
7. J. E. ASHTON, J. C. HALPIN and P. H. PETIT, “Primer on Composite Materials: Analysis” (Technomic, Lancaster, Pennsylvania, 1969) p. 35.
8. A. KELLEY and J. G. DAVIES, *Metals Rev.* **10** (1965) 1.
9. P. W. JACKSON and D. CRATCHLEY, *J. Mech. Phys. Solids* **14** (1966) 49.
10. G. A. COOPER, *ibid.* **14** (1966) 103.
11. R. HILL, “The Mathematical Theory of Plasticity” (Clarendon, Oxford, 1950) p. 317.
12. S. W. TSAI, in “Fundamental Aspects of Fibre Reinforced Plastic Composites”, Vol. 3, edited by R. T. Schwartz and H. S. Schwartz (Interscience, New York, 1968) p. 3.
13. *Idem*, “Strength Characteristics of Composite Materials”, NASA CR-224 (NASA, Washington, D.C., 1965).

*Received 11 February  
and accepted 29 April 1987*